

Contract No.:

This manuscript has been authored by Battelle Savannah River Alliance (BSRA), LLC under Contract No. 89303321CEM000080 with the U.S. Department of Energy (DOE) Office of Environmental Management (EM).

Disclaimer:

The United States Government retains and the publisher, by accepting this article for publication, acknowledges that the United States Government retains a non-exclusive, paid-up, irrevocable, worldwide license to publish or reproduce the published form of this work, or allow others to do so, for United States Government purposes.

Imaginary Admittance and Charge Transfer Resistance Correlate to the Physiological Status of *Shewanella oneidensis* Cultures in Real Time

Hunter R. Teel¹, K. Likit-anurak¹, Sirivatch Shimpalee¹, and Charles E. Turick^{*2,3}

¹University of South Carolina, Columbia, SC, USA,

²Savannah River National Laboratory, Aiken, SC, USA,

³ElectroBioDyne LLC, Aiken, SC, USA

ABSTRACT

Monitoring microbial activity is essential for industrial and environmental applications to proceed efficiently. To minimize time and labor-intensive monitoring, a new paradigm is required for in-situ, real time analysis. Since bioconversion of organics is accomplished by microorganisms through the oxidation of feedstocks linked to the reduction of electron acceptors, microorganisms can be viewed as electrochemical catalysts. In this respect, cell membranes have an electrical potential, which is analogous to a conventional capacitor and linked dynamically to cellular activity. Here we demonstrate the use of electrochemical impedance spectrometry (EIS) and cyclic voltammetry (CV) for monitoring microbial metabolic activity in real time, in-situ. The effect of organic electron donors as a function of concentration to the physiological status of strains of *Shewanella oneidensis* was determined. In this study, the pyomelanin overproducer (*S. oneidensis* $\Delta hmgA$) and the pyomelanin deficient mutant (*S. oneidensis* $\Delta melA$) were chosen due to different surface electrochemical characteristics along with differences in oxygen utilization efficiency. CV, relative admittance, phase shift and permittivity changed with growth status and correlated with electron flow from organic carbon sources and terminal electron acceptor availability. This work offers a novel and inexpensive approach to real time monitoring with the advantage of abundant data.

Keywords. In-situ monitoring, Cyclic voltammetry, Electrochemical impedance spectroscopy, Charge transfer resistance, *Shewanella*

Hunter Teel
College of Engineering and Computing
541 Main Street
Columbia, SC 29208
HTEEL@email.sc.edu

Kris Likit-anurak
College of Engineering and Computing
Horizon 1
541 Main Street
Columbia, SC 29208
KRISL@email.sc.edu

Sirivatch Shimpalee
College of Engineering and Computing
Horizon 1
Room 439
541 Main Street
Columbia, SC 29208
SHIMPALE@cec.sc.edu

*Charles E. Turick
ElectroBioDyne, LLC
308 Hopeland Farm Dr.
Aiken, SC 29803
ElectroBioDyne@gmail.com
1-803-552-9508

*Corresponding author

1. Introduction

Microbial cell membranes have an electrical potential difference analogous to a conventional battery that is linked dynamically to cellular activity. Such electrochemical cellular processes include membrane potential, redox metabolism, and extracellular electron transfer and/or uptake [1,2]. As a result, cellular electrochemical phenomena can be incorporated into simple equivalent circuits to define physiological dynamics [2]. By regarding microbes as sensors or batteries, electrochemical techniques can be used to gather information about their physiological status, remotely and in real time. This leads to an emerging new paradigm in linking electrochemistry to remote monitoring of microbial physiology and growth status.

In-situ electrochemical methods offer significant opportunities in monitoring cell physiology with benefits for a variety of biotechnological applications including biofilm analysis, industrial bioprocessing, biomining, and bioremediation [3-5]. When a small AC voltage is applied to a growth medium with cells, electrical conduction is faster through the medium than lipid bilayers of cell membranes, making the current lag behind the voltage and causing a phase shift [6]. In addition, the flow of ions around the cell membrane responds to various frequencies as a function of activity and growth status. These parameters change throughout the cellular growth cycle and reflect factors related to biomass density, cell viability, membrane integrity, and the overall metabolic state of microbes [7-9].

Electrochemical impedance spectroscopy is a technique that provides information about specific cellular biophysical parameters at a range of specific frequencies as well as the holistic interrogation of parameters across a wide frequency range. The tremendous advantage of this label free monitoring technique is that the inherent complexity of data across several logs of frequency offers the capability of delivering specific information regarding numerous multifaceted parameters, like changes in fluid composition (conductivity, reaction, and diffusion rates); microbial density, metabolic activity, and growth status during each scan. These parameters change throughout the cellular growth cycle and reflect factors related to biomass density, cell viability, membrane integrity, and the overall metabolic state of microbes [7-9]. Cell size also plays a factor with greater sensitivity as a function of cell size [10]. Impedance techniques are also insensitive to dead cells and non-cellular matter [3,11] hence, are well suited to monitor living cells.

Frequency range is important to consider. Biological materials behave differently at different frequencies where their conductivity increases in a step wise manner (known as dispersions) with increasing frequency while permittivity (a property of capacitance) decreases with increasing frequency [12]. The steps are referred to as α , β , and γ dispersions, where α -dispersions are generally associated with the diffusion processes of ionic species due to the tangential flow of ions across cell surfaces. β -dispersions relate to interfacial polarization across the cellular plasma membranes and their interactions with the extra and intra-cellular electrolytes, while γ -dispersions are at the higher range of frequencies in biological materials and are due to the dipolar rotation small molecules, particularly water [10, 13]. When live cells are placed in time oscillating electric fields, these charges move on the surface of the membrane, giving rise to high polarizations (α effect). As the mobility of these surface charges is relatively small, this effect is manifest at low frequencies, such that the relative dielectric permittivity of live cell suspensions can be as high as 10^6 [14, 15]. The β relaxation is related to the dielectric structure of the cell's membrane itself and can enhance the dielectric permittivity at higher frequencies [16]. The focus of this current work was between 100 kHz and 10 mHz, within the

range of α and β dispersions and focused on changes in permittivity and admittance as a function of growth.

When a range of frequencies are analyzed together as one spectrum, data can be modeled by an equivalent circuit to further define the microbe as an electrical entity and can provide information about the medium conductivity, and charge transfer resistance that is directly linked to cellular physiological activity [17,18]. Previous work demonstrated the use of electrochemical techniques, including cyclic voltammetry, to monitor the physiological activity of the Gram-positive organism *Clostridium phytofermentans* [17]. Cyclic voltammetry provides additional information related to cellular redox behavior [4, 19].

The present study used the Gram-negative *Shewanella oneidensis* due to its outer membrane cytochromes [20] as this may provide a model electrochemical monitoring system. Two deletion mutants were used for this work. *S. oneidensis* $\Delta hmgA$, a pyomelanin overproducer and the pyomelanin deficient mutant *S. oneidensis* $\Delta melA$ [19]. Pyomelanin is an electroactive quinoid polymer capable of accepting electrons and is easily oxidized by other terminal electron acceptors, including O_2 . When pyomelanin is associated with the cell surface [19, 21, 22] the cell demonstrates no loss of viability [23] and demonstrates enhanced electron transfer and thus metabolic activity. Low dissolved O_2 levels of $1.74 (\pm 0.085) \text{ nM mL}^{-1}$ [19] were previously reported for high cell density cultures of aerobically grown *Shewanella oneidensis*. Hence, these strains were used to differentiate physiological and biophysical conditions during aerobic growth as dissolved O_2 conditions declined when grown on glucose followed by supplemental addition of glucose.

The main objective of this work was to use EIS to demonstrate a decrease in admittance values as electron donor concentrations decline during growth in batch culture and a rapid increase in admittance in response to the addition of a fresh source of electrons. An additional objective was to show a concomitant increase in charge transfer resistance as electron donor concentrations decline and a rapid decrease in charge transfer resistance can easily be detected as soon as a source of electrons is added to a growing culture.

2. Materials and Methods

2.1. Growth study.

2.1.1 Cultures

Knock out mutants of *S. oneidensis* MR-1 that overproduce pyomelanin ($\Delta hmgA$) and a pyomelanin deficient strain ($\Delta melA$) [19] were used in this study.

2.1.2 Growth conditions

Cultures adapted to growth with glucose as sole carbon and energy source [24] were used throughout the study. Cultures were pregrown in 20 ml tryptic soy broth (TSB) at 25°C for 48 h, to stationary phase growth and maximum pyomelanin production [19]. For respirometry studies Bushnell-Haas medium (BHM) was used as a low nutrient minimal medium and supplemented initially with 15 g L^{-1} glucose. Sterile glucose (15 g L^{-1}) was added again after 42 hours of growth to cultures at 25°C , stirred at 50 rpm with magnetic stir bars in order to maintain cells in suspension. The second glucose addition served as a supplemental electron donor in order to

determine the electrochemical response of the cultures. Magnetic stirring did not affect electrochemical results. Inocula from each strain consisted of two, 20 ml cultures of centrifuged (5000 g) washed (sterile BHM) added to the BHM with glucose for a 20% inoculum in 200 ml BHM + glucose for respirometry/electrochemistry studies.

2.1.3 Respirometry

Glass vessels retrofitted with side arms for aseptic sampling and Viton rubber stoppers to contain flat patterned electrodes were used in this study (Supplemental information S1). Sterile vessels with stir bars and caps fitted for respirometer tubing were filled with 200 ml sterile BHM + glucose prior to the first electrochemical assays.

Respirometry was conducted with the Columbus Instruments Micro-Oxymax Respirometer, a closed-circuit system capable of measuring O₂ gas consumption and CO₂ gas production with a sensing threshold at 0.2 microliters per hour. O₂ concentrations were maintained at 20% in the headspace throughout the study. The difference in gas concentrations along with flow information was employed to calculate oxygen consumption and carbon dioxide production. All data were corrected to a STP of 0°C and 760 mmHg.

Alterations in headspace volume were minimized and only occurred with the addition of 5 ml of concentrated sterile glucose immediately following removal of 5 ml of spent medium at 42 hours of incubation. An identical study was conducted in parallel in order to collect samples for cell densities (OD₆₀₀) and glucose concentration (electrochemical glucose sensor). High cell density necessitated a 10⁻¹ dilution in sterile PBS for OD measurements and converted to mg mL⁻¹ based on previous growth data (Supplemental information S2).

2.2 Electrode configuration

Flat patterned electrodes (Pine Instruments) consisted of a 2 mm diameter graphite working electrode surrounded on 3 sides by a graphite counter electrode with a Ag/AgCl reference electrode. Electrodes as described previously were fitted through preformed slits in butyl rubber stoppers for gas tight closure and secured into serum vials with aluminum seals [17].

2.3 Glucose analysis

Parallel cultures were conducted in three identical vessels as the electrochemical studies (above) and sampled (1 ml) (in triplicate) for glucose concentrations and cell densities throughout growth. Following centrifugation (5000g), the supernate was diluted 10X for electrochemical analysis as previously described [25]. Samples (100 µl) were placed on an amperometric glucose oxidase three-electrode sensor (BVT-AC1.GOx Glucose sensor) and monitored at 250 mV with a PalmSens³ potentiostat.

2.4 Cyclic voltammetry

All electrochemical studies were performed on a two channel potentiostat, SP-300 (Biologic) with data recorded via EC Lab software version 10.37. Cyclic voltammetry (CV) was used to monitor changes in the electrochemistry of the system during the growth and uninoculated medium. Throughout the studies, the flat patterned graphite electrode was first

electrochemically cleaned to remove any fouling on the electrode (including biofilm development) by sweeping the potential rapidly from -2.0 to $+2.0$ V at 1 V s^{-1} for electrochemical cleaning with at least three cleaning scans before each analysis (Martin et al. 2018) (Supplemental information S3). The CV of the final cleaning scan was compared to that of bare electrodes to confirm fouling was not present. CV and EIS analyses (scan rate 25 mV s^{-1}) of cell suspensions were conducted about every 3 hours during the study. Analysis of CV data was accomplished with the provided software to determine peak currents and charge density associated with bacterial growth stages.

2.5 EIS

Prior to this study, stability of EIS measurements over time with sterile medium were determined as well as data quality under growth conditions (Supplemental information S4) to demonstrate the utility and precision of this analytical technique. Throughout this study, and following each CV scan, EIS measurements were carried out in sterile and inoculated media with a sinusoidal signal perturbation of 50 mV , with a frequency range of 10^5 Hz to 10^{-2} Hz . Ten measurements were recorded per decade of frequency with a measurement delay of 2 s . Data were analyzed with ZView software (Scribner Associates). Relative values (Δ) were determined by subtracting initial values of inoculated media taken at the beginning of each study and at the second addition of glucose.

2.6 Data analysis and description

Data were evaluated as Nyquist and Cole–Cole plots. The Nyquist plot represents impedance at each frequency, $Z(\omega)$, in complex plane where real (Z') and imaginary (Z'') impedance are measured. The complex dielectric function [28] was presented as Cole–Cole plots where real (ϵ') and imaginary (ϵ'') permittivity are a function of impedance as defined follows:

$$\epsilon' = \frac{-Z''}{(Z'^2 + Z''^2)\omega C_0} \quad (1)$$

$$\epsilon'' = \frac{-Z'}{(Z'^2 + Z''^2)\omega C_0} \quad (2)$$

where ω = angular frequency and C_0 = capacitance of an empty cell.

Permittivity (ϵ) has been linked to cellular proton gradients and thus cell viability [15, 16, 26]. Here we measured real relative permittivity by the ratio of ϵ'/ϵ_0 where ϵ_0 is the permittivity of a vacuum ($8.85 \times 10^{-12}\text{ F m}^{-1}$). Data at 0.1 Hz were plotted over time to provide an understanding of proton gradients.

Impedance can be viewed as a very complex type of resistance. In a simple DC system resistance has an inverse relationship to conductivity. With impedance being similar to resistance, admittance (Y) is similar to conductivity and measured in Siemens. Admittance (Y) has been correlated to cellular activity [27]. Here we used imaginary admittance (Y'') and is defined as:

$$Y'' = \frac{-Z''}{Z'^2 + Z''^2} \quad (3)$$


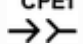
Y'' can also be defined as Seamans per meter, which is then termed σ'' and defined as:

$$\sigma'' = Y'' \frac{d}{a} \quad (4)$$

with d = distance between electrodes and a = effective area of the electrode.

2.6 Circuit model and description of parameters

Electrochemical data from this work incorporated the entire spectrum of frequencies to obtain information about various parameters simultaneously. This involved the complex dielectric function presented where Z'' is plotted over Z' (Nyquist) or Cole-Cole plots where ε'' is plotted over ε' [28]. The resulting data from these analyses were then interpreted using a circuit model (Fig. 1) to determine electrochemical parameters relevant to microbial activity throughout the growth cycle.

Impedance and permittivity data from EIS analyses were interpreted using the circuit model below (Fig. 1) to determine electrochemical parameters relevant to microbial activity throughout the growth cycle. For circuit model development the elements are sized using a Complex Non-linear Squares (CNLS) method to give the best fit of the equivalent circuit model to the experimental data. Typical electric circuits used to model impedance data are resistor (zero frequency impedance, R ) and constant phase element (CPE ).

Insert figure 1 here

3. Results and discussion

3.1 Growth study

The pyomelanin overproducer *S. oneidensis* $\Delta hmgA$ and the pyomelanin deficient strain *S. oneidensis* $\Delta melA$ were grown in a minimal medium to evaluate electrochemical parameters as a function of growth dynamics during oxygen stress and carbon and energy source use and supplementation.

3.1.2. Electron donor and acceptor utilization and cell density

Carbon source and O_2 utilization coincided with CO_2 yield and increasing cell density. O_2 utilization and CO_2 production increased immediately following glucose supplementation around 42 hours (Fig. 2). Differences between strains are indicative of the respiratory advantage of strain $\Delta hmgA$ provided by pyomelanin. Pyomelanin can serve as a terminal electron acceptor, as this electroactive quinoid polymer is an easily accessible reservoir of electrons or temporary electron sink [22,29]. One fg of cell associated pyomelanin per cell contains sufficient electron

storage capacity to support the electron flow needed by a cell for up to 16 min. when electron donors or electron acceptors become temporarily unavailable, and respiration rate is low [22]. Based on a previous report [19], growth conditions in TSB resulted in >100 fg pyomelanin per cell at the beginning of this study. Consequently, the *ΔhmgA* strain had sufficient electron acceptor capacity to overcome diminished O₂ concentrations resulting from high cell density. Conversely, the pyomelanin deficient strain, *ΔmelA* demonstrated lower respiratory activity, especially following glucose supplementation after 42 h.

Insert figure 2 here

3.1.3 Phase shift

Electrochemical characteristics of the cell surface can be attributed to surface chemistry as well as the physiological dynamics of the cell membrane such as electron flow and proton gradients. Overall, $\Delta\phi$ peaks increased in magnitude (degrees) during microbial growth (Fig. 3). This is attributed to the increase of biomass and therefore an increase in lipid membranes that results in the magnitude of the phase shift, ($\Delta\phi$) [6, 10]. However, the peaks were evident at different frequencies throughout growth with a trend toward decreased frequencies as growth slowed. This trend is elucidated in Figure 4 where maximum peak heights and frequencies are plotted.

Insert figure 3 here

The phase shift relates to differences between the cell surface relative to the conductivity of the medium. This is in part a result of the lower electrical resistance of cellular lipid membranes [6]. In this case $\Delta\phi$ was more pronounced for the pyomelanin deficient strain *ΔmelA*. Since pyomelanin is conductive and changes the electroactive properties of the cell surface [22, 29] the increased surface conductivity provided to *ΔhmgA* by pyomelanin resulted in the lower values for $\Delta\phi$ peak heights during growth, relative to *ΔmelA*.

Insert figure 4 here

As growth rates decline and membrane dynamics slow, a decrease in the frequency of electrochemical activity was anticipated. Immediately following the supplementation of glucose after 42 h growth, changes in peak heights and maximum peak frequencies were evident from both strains (Fig. 4). It is important to note that cell densities for both strains correlated well with $\Delta\phi$ up to glucose supplementation (Fig. 4 insets). Following glucose addition, cell density values deviated from those of $\Delta\phi$. Likely, changes in the cell surface charges contributed to these changes. The prolonged change in *ΔhmgA* (Fig. 4a) may be a result of increased surface conductivity possibly linked to electron flow to pyomelanin during high cell density at this stage of the culture. In contrast, $\Delta\phi$ values of the pyomelanin deficient mutant (*ΔmelA*) only diverged from their correlation to cell density immediately after glucose supplementation (Fig. 4b, inset). This may be a result of changes in cell surface polarization [30].

3.1.4. Real relative permittivity

Permittivity (ϵ) is linked to cellular proton gradients and thus cell viability [15, 16, 26]. Here we measured the change of real relative permittivity ($\Delta\epsilon'/\epsilon_0$) and also demonstrated a link to metabolic activity as measured by CO₂ yield (Fig. 5). Following the second glucose addition (42 h), real, relative permittivity increased along with CO₂ yield for the respiratory robust strain (*ΔhmgA*) (Fig. 5a). However, $\Delta\epsilon'/\epsilon_0$ values dropped markedly, shortly after the second glucose addition in the culture with impaired respiratory capabilities (*ΔmelA*) and coincided with a cessation of CO₂ production (Fig. 5b). When an uptake system is derepressed by starvation, as in this case with *ΔmelA*, the addition of glucose can cause a large depolarization of the membrane as well as a brief, net uptake of protons where the uptake of protons corresponds proportionally to the ratio of H⁺:sugar [30]. Both the proton uptake and the depolarization decrease with time, presumably due to a speeding up of the H⁺- efflux pump [2].

Insert Figure 5 here

3.1.5. Admittance

Admittance (Y'') represents the polarization (*energy storage*) term expressed in Seimans (S) or as σ'' when expressed in S m⁻¹ [31]. Here, *S. oneidensis ΔhmgA*, and *S. oneidensis ΔmelA* demonstrated multiple peaks between 1 Hz and 100 Hz during growth studies with peak heights generally increasing during increased growth when additional carbon and energy sources were administered (Fig. 6). Previous studies have also correlated trends in bacterial growth to increased values of Y'' [32] or σ'' associated with only single additions of carbon and energy sources [26, 31, 33-35].

The frequencies of the peaks in the present study varied with time and physiological activity based on glucose concentration (Fig. 6). Mellage et al. [34], demonstrated similar trends with σ'' in peak values and peak frequency shifts with column studies of *S. oneidensis* due to transient inhibitory concentrations of NO₂, ascribed to changes in cell surface charging.

When peak heights and frequencies of $\Delta Y''$ were plotted over time, these values gradually declined following initial addition of glucose with sharp increases immediately following glucose supplementation after 42 h (Fig. 7).

Average $\Delta Y''$ peak heights (and SD) during 3 hours prior to glucose addition for *ΔhmgA* was 9.24×10^{-5} S (1.0×10^{-6}) compared to 1.70×10^{-4} S (2.1×10^{-6}) during the 3 hours immediately after glucose addition. Similarly, $\Delta Y''$ peak heights 3 hours prior to glucose addition for *ΔmelA* were 8.36×10^{-6} S (5.7×10^{-7}) compared to 4.9×10^{-5} S (3.6×10^{-6}) for 3 hours immediately after glucose addition. $\Delta Y''$ peak frequencies also demonstrated increased values with *ΔhmgA* with 31.6 Hz (0) before glucose supplementation and 71.3 Hz (11.5) after. Average $\Delta Y''$ peak frequencies for *ΔmelA* were 1.3 Hz (0.22) for 3 hours prior to glucose addition and 10 Hz (0) after addition.

Overall, $\Delta Y''$ followed O₂ and glucose utilization (Fig. 2) with *S. oneidensis ΔhmgA* displaying greater physiological robustness, ascribed to the electron transfer capacity of surface associated pyomelanin. Following glucose supplementation, *S. oneidensis ΔmelA* demonstrated a sharp increase in O₂ and glucose utilization along with CO₂ production but for only a few hours.

Decreased O₂ availability due to high cell density along with diminished electron transfer capacity and minimal nutrient conditions likely contributed to the physiological decline of this culture. This is also evident in the sharp increase in maximum peak heights and frequencies after glucose supplementation (Fig 7b). In contrast *S. oneidensis* $\Delta hmgA$ demonstrated decreased maximum $\Delta Y''$ peak heights and frequencies as a function of glucose concentration which resulted in a decreased metabolic rate as evidenced in lower O₂ utilization as glucose concentrations declined (Figure 2a and 2c). The sudden increase in $\Delta Y''$ values directly after glucose supplementation followed by sustained values along with O₂ and glucose utilization correlates well with $\Delta Y''$ as an indicator of cellular metabolic status as related to membrane potential in *Shewanella*. Pribadian et al. [36], also demonstrated that membrane potential is strongly associated with electron acceptor availability. In that respect, in this study the permittivity data here (Fig. 5) ascribed to membrane depolarization in *S. oneidensis* $\Delta melA$ correlated to $\Delta Y''$ (Fig. 7).

Insert Figure 6 here

Insert Figure 7 here

3.1.6. Nyquist plots

In the low frequency region of the Nyquist plots (Fig. 8), both *S. oneidensis* $\Delta hmgA$, and *S. oneidensis* $\Delta melA$ show a decrease in the low frequency impedance from the beginning of the experiment until the glucose addition at 42 hours. This correlates to the increase in the admittance peak heights during the time of growth. The imaginary portion of the impedance for *S. oneidensis* $\Delta melA$ also has a greater magnitude than *S. oneidensis* $\Delta hmgA$ indicating that the imaginary portion of impedance corresponds to capacitive elements. For the low frequency range (right side of Nyquist) where there is high imaginary impedance, the constant phase elements (CPEs) (discussed in section 3.1.8) dominate the fitting due to the relationship between capacitance and the imaginary impedance. This may indicate that *S. oneidensis* $\Delta melA$ experiences greater impedance compared to *S. oneidensis* $\Delta hmgA$ due to differences of the capacitive elements of its physiology, such as the electric double layer at the outer membrane resulting from the presence of pyomelanin. For both mutants the low frequency impedance was relatively stable after 17.5 hours. This indicates a decrease in growth of the cells or the established path of electron flow in the outer membranes. After glucose addition at 42 hours, the impedance for *S. oneidensis* $\Delta hmgA$ decreased continuously until the end of the experiment while *S. oneidensis* $\Delta melA$ slightly decreased at 51.5 hours before increasing until the end of the experiment at 62 hours. In addition, for *S. oneidensis* $\Delta melA$ there was a significant increase in the real part of complex impedance, indicating that values for at least one of the resistors was increasing significantly during this time. The increase in real impedance correlates to an increase

in charge transfer resistance, which is visible on the Nyquist plots and through its representative resistor in the circuit, R3.

The high frequency portion of the Nyquist plots depicted in the inserts show that the magnitude of the impedance for both *S. oneidensis* $\Delta hmgA$, and *S. oneidensis* $\Delta melA$ in this portion slightly increases with time. The charge transfer resistance, which is defined by the local minimum of the Nyquist plots in the high frequency portion, also continuously increased until glucose addition. This indicates an increase in difficulty to transfer charge to the terminal electron acceptor in relation to decreased cellular growth rates. Immediately after glucose addition, there is a sharp decrease in the impedance close to the value of the 0-hour impedance. The charge transfer resistance also sharply decreases, as the introduction of the carbon source changes the gradient as more charges are available. Shortly after the glucose addition for *S. oneidensis* $\Delta hmgA$, the impedance and charge transfer resistance remained relatively constant in the high frequency domain with a slight decrease in the impedance as time went on. However, in regard to *S. oneidensis* $\Delta melA$, while there was a temporary decrease in impedance from the glucose addition, the impedance rapidly grew larger than it had been before. The physiological differences between the mutants are likely the cause of this difference as *S. oneidensis* $\Delta hmgA$ was able to stabilize the charge transfer process likely with an established electron transport system while *S. oneidensis* $\Delta melA$ electron transport system quickly failed and destabilized, likely due to decreased access to the terminal electron acceptor.

Insert Figure 8 here

3.1.7. Cole-Cole plots

The Cole-Cole plots depicted in Figure 9 show the real and imaginary relative permittivity of the system. For the first several hours, the permittivity is almost identical for both *S. oneidensis* $\Delta hmgA$ and *S. oneidensis* $\Delta melA$. After about 10 hours, the permittivity for *S. oneidensis* $\Delta hmgA$ grows faster than *S. oneidensis* $\Delta melA$. Between 17.5 hours until glucose addition, there are relatively small changes in the permittivity. The imaginary portion of the relative permittivity for *S. oneidensis* $\Delta hmgA$ is much greater than *S. oneidensis* $\Delta melA$, and similarly, the real part of the relative permittivity is greater for *S. oneidensis* $\Delta melA$ than *S. oneidensis* $\Delta hmgA$. Immediately after glucose addition, both strains show a decrease in the permittivity with *S. oneidensis* $\Delta melA$ experiencing a greater drop. Shortly after glucose addition, the relative permittivity for *S. oneidensis* $\Delta hmgA$ increases slightly with the greatest portion of growth occurring with the real part of the relative permittivity. For *S. oneidensis* $\Delta melA$, shortly after glucose addition the relative permittivity increases greatly, with much of the growth occurring with the imaginary portion of relative permittivity.

Insert Figure 9 here

3.1.8 Equivalent circuit analysis

In the equivalent circuit model, the first resistor- circuit element R1- relates to the resistances introduced by the solution and electrodes. Compared to the other resistances introduced by the microbes, R1 demonstrated expected minor fluctuations occurring as

molecules are introduced into the solution (Fig. 10). During cell growth between 0 and about 16 hours, minor changes in R1 values were detected in the *ΔhmgA* culture medium as small fluctuations in resistance.

Insert Figure 10 here

Insert Figure 11 here

R2 values regarding bacterial activity were previously ascribed to extracellular processes [37], such as ionic flux across the outer membrane, for instance the biophysical activities associated with spore germination [17]. Secretion of extracellular electron shuttles by *Shewanella* are involved in electron transfer to solid terminal electron acceptors like Fe (III) oxides under anaerobic conditions but are also produced in just as high a concentration (2.9 and 2.1 μmol per gram of cellular protein) during aerobic growth [38]. Extracellular mediators contribute to changes in impedance in bacterial systems [39]. In the present study R2 parameters (Fig. 11) may be linked, at least in part to the rate of secretion of extracellular electron shuttles like quinones [40] and more specifically flavins [38, 41, 42]. The lower R2 values exhibited by *S. oneidensis ΔhmgA* are as much as 3 logs lower than the pyomelanin deficient strain *S. oneidensis ΔmelA* and likely due to the enhanced electron transfer capacity provided by pyomelanin. *S. oneidensis ΔmelA* may need to produce electron shuttles than *S. oneidensis ΔhmgA* as a result of its electron transfer deficiency. However this hypothesis is beyond the scope of this study and represents targets for further investigation. Although EIS can be used to demonstrate the contribution of biologically secreted electrochemical mediators it cannot provide detail on types or chemical properties [39].

Insert Figure 12 here

In the equivalent circuit model, the third resistor- circuit element R3- relates to the charge transfer resistance and carbon source utilization and was previously ascribed to intracellular reaction steps involved in extracellular electron transfer [37]. For both *S. oneidensis ΔhmgA* and *S. oneidensis ΔmelA*, as growth occurred for the microbes, the value for R3 increased (Fig. 12). The values for circuit element R3 continue to increase until the second glucose addition at 42 hours. At this point, both *S. oneidensis ΔhmgA* and *S. oneidensis ΔmelA* experience a drop in the

R3 resistance. This trend is similar to the high frequency region observed in the Nyquist Plots (Fig. 8) previously, where the microbes show an increase in resistance/ impedance until the second glucose addition. The comparison of Figure 12 to Figure 8 continues as values for impedance and resistor R3 remain constant for *S. oneidensis* $\Delta hmgA$ while *S. oneidensis* $\Delta melA$ shows a large increase in resistances shortly after the second glucose addition. Referring to the high frequency inserts of Figure 8, the increase in impedance for *S. oneidensis* $\Delta melA$ during growth also appears to be at a greater magnitude than that of *S. oneidensis* $\Delta hmgA$ which is reflected here in Figure 12 as the difference in magnitude of the resistor R3 values. From these trends, it's likely that circuit element R3 corresponds to the charge transfer resistance of the microbes. The high frequency portion of the Nyquist Plots where charge transfer resistance is depicted and the values for R3 match well.

The P components of both CPEs remain relatively stable with values lower than 1. This component compensates for the differences between a capacitor and a double layer such as the cell membranes. The T component shows the changes in capacitance in farads over time. CPE1 demonstrated interesting behavior with relatively stable values from the beginning of data collection until 30 hours of incubation, when less glucose is present. The value for $\Delta hmgA$ CPE1-T increases from 32 hours until the end of data collection at 62 hours, with a momentary dip occurring at 41.5 hours when glucose is added. $\Delta melA$ CPE1-T doesn't experience an increase in value until the hours after glucose addition where there is an increase before decreasing again at 51.5 hours. The changes in the CPE1-T values might be attributed to the cells using a method of exchanging electrons at the cell membranes, for instance pyomelanin in the case of $\Delta hmgA$. The changes in circuit element R2, which is attributed to the secretion of extracellular electron shuttles, appear to vary slightly with CPE1-T. After 41.5 hours for $\Delta melA$, there is an increase in CPE1-T and a decrease in R2 until 51.5 hours where CPE1-T decreases and R2 increases again. For $\Delta hmgA$, the initial growth of R2 is mirrored by an initial decrease in CPE1-T. However, CPE1-T grows significantly larger for $\Delta hmgA$, especially after the glucose addition at 41.5 hours which may indicate that electron transfer primarily at the cell membrane. The CPE1-T values also change with R3 which is attributed to charge transfer resistance. When resistance decreases, the capacitance tends to increase. CPE2-T grows steadily for both $\Delta hmgA$ and $\Delta melA$. Due to the position of CPE2 in the circuit (series to R3), CPE2 functions more as just a fitting parameter.

3.1.9. Cyclic Voltammetry

CVs of *S. oneidensis* $\Delta melA$ suspensions (Fig. 14) demonstrated minimal change throughout the study until the end of the study when cellular activity diminished substantially and CVs revealed minimal electrochemical activity (Fig. 14d). CVs of *S. oneidensis* $\Delta hmgA$ suspensions however changed during growth conditions. In the presence of higher electron donor concentrations (Fig. 14a and 14c) $\Delta hmgA$ demonstrated increased current at the lower potential. These CV data coincide with the increase of resistances depicted in Figure 12 along with the increase of impedance observed in the Nyquist plots (Fig. 8), and indicate that the microbe's electrochemical activity diminished significantly as glucose concentrations declined.

Additionally, the decrease in oxygen usage by *S. oneidensis* $\Delta melA$ depicted in Figure 2 corroborates that *S. oneidensis* $\Delta melA$ loses some ability to exchange electrons and reduce/oxidize species thereby resulting in impeded growth. *S. oneidensis* $\Delta hmgA$ shows the opposite of this, as redox activity increased (Fig. 14d). The ability of *S. oneidensis* $\Delta hmgA$ to continuously oxidize and reduce species allows the microbe to grow more effectively while minimizing the resistances of the system can be attributed to surface associated pyomelanin. Increased electron transfer to the cell surface by $\Delta hmgA$ later in this study (Fig. 14d) coincides with increased surface conductivity as demonstrated in a decrease in $\Delta\phi$ values (Fig. 4a) as well as previous CV studies demonstrating the electroactive contribution to the cells by pyomelanin at high cell density [19].

Insert Figure 14 here

Summary and Conclusions

Here we demonstrate correlations between electrochemical activity when physiological status in batch cultures was followed during glucose utilization and repeated during glucose supplementation. This is notable because rapid increases in cellular activity (immediately following carbon and energy source supplementation) were detected electrochemically in real time. EIS conducted at frequencies of 100 kHz to 10 mHz provided a means of monitoring microbial physiological status, in-situ and in real time without the need for sample acquisition. Admittance values (including magnitude and peak frequency) spiked as a function of faster growth responding to increased electron donor abundance.

A significant advantage of using electrochemical techniques is the abundance of data that can be obtained from scans that represent a holistic view of physiological status. For instance, cell density as a function of the phase shift of the signal was possible. As cell density increased during the first addition of electron donor the phase shift values increased as well due to the increased cellular lipid component in the medium and hence increased impedance of viable cells. Differences in the conductivity of the cell surface resulted in differences in phase data but a general trend to increase with cell density was evident. Upon supplementation of the electron donor about mid-way into the growth study, changes in the phase data were evident and ascribed to changes in cell polarization. Consequently, understanding the influence of one parameter on the others is important for a comprehensive evaluation of metabolic activity.

Changes in proton gradients, ascribed to real relative permittivity data were also evident and followed cellular growth status. The use of equivalent circuits provided another means of data analysis by quantifying charge transfer resistance in these cultures as a function a decreasing source of electrons (glucose). Nyquist plots reponed to changes in cellular impedance and Cole-

Cole plots followed permittivity changes. Both were responsive to physiological status as a function of glucose utilization and demonstrated clear trends of increasing charge transfer resistance as cellular activity declined. In addition to EIS, CV provided valuable data regarding the redox status of cells.

This work has expanded on previous studies in this field by evaluating impedance parameters with a holistic approach and highlighted their complex interrelationships, especially since electron donor supplementation was also studied. Future research will be designed to quantitatively evaluate specific metabolic parameters (i.e. $\Delta\phi$, $\Delta Y''$ and $\Delta\epsilon'/\epsilon_s$) and will require statistical evaluation beyond provisional use of pseudo-replicate measurements as in the present work.

Obtaining precise electrochemical measurements from batch studies of pure cultures presents a challenge partly due to inherent metabolic variability from clonal phenotypic heterogeneity [43, 44] and to a greater degree to transient growth conditions in batch cultures. This transience refers to factors like carbon and energy sources declining during growth, increasing cell density, changes in medium composition like pH and fluid conductivity, production of metabolic byproducts and secondary metabolites. These changes can contribute significantly to variability of electrochemical parameters and should be controlled when possible.

This challenge can be addressed without changing medium composition or operating conditions by poising growth at specific rates through continuous culture techniques [45]. This approach will provide an opportunity to isolate and define quantitative electrochemical parameters such as $\Delta\phi$, $\Delta Y''$ and $\Delta\epsilon'/\epsilon_s$, relative to cell density and growth status during well controlled growth conditions. In addition, disruption of cell growth, electron transfer and proton gradients through the use of metabolic uncouplers [46, 47] will provide utility in defining and quantifying specific growth parameters. This work offers potential for remote in-situ monitoring of microbial activity related to environmental monitoring and industrial applications. Electrochemical monitoring may also be linked to automated bioprocess control through machine learning.

Funding

This research was supported by the Savannah River National Laboratory through the Laboratory Directed Research and Development Program, Strategic Initiative. This document was prepared in conjunction with work accomplished at SRNL under Contract No. DE-AC09-08SR22470 with the U.S. Department of Energy.

Acknowledgments

The authors would like to acknowledge the computational work of Michael Laird, Blake DeVivo's contribution to electrochemical cleaning and the excellent technical assistance of Courtney E. Burckhalter and the late Charles E. Milliken.

References.

- [1] J.M. Benarroch, M. Asally, The microbiologist's guide to membrane potential dynamics, *Trends in Microbiology*, 28 (2020) 304-314, doi:10.1016/j.tim.2019.12.008.
- [2] R.J. Poole, Energy coupling for membrane transport. *Ann. Rev. Plant Physiol.* 29 (1978) 437-60.
- [3] J.P. Carvell, J.E. Dowd, On-line measurements and control of viable cell density in cell culture manufacturing processes using radio-frequency impedance, *Cytotechnol.* 50 (2006) 35-48, <https://doi.org/10.1007/s10616-005-3974-x>.
- [4] C.E. Turick, P. Satjaritanun, S. Shimpalee, J. Weidner, S. Greenway. Convenient non-invasive electrochemical techniques to monitor microbial processes: current state and perspectives. *Appl. Microbiol. Biotechnol.* 103 (2019) 8327–8338, <https://doi.org/10.1007/s00253-019-10091-y>.
- [5] G. Flores-Cosío, E. Herrera-López, M. Arellano-Plaza, A. Gschaedler-Mathis, M. Kirchmayr, L. Amaya-Delgado, Application of dielectric spectroscopy to unravel the physiological state of microorganisms: current state, prospects and limits. *Applied Microbiology and Biotechnology*, 104 (2020) 6101-6113, DOI:10.1007/s00253-020-10677-x.
- [6] H. Cichoż-Lach, A. Michalak, A Comprehensive review of bioelectrical impedance analysis and other methods in the assessment of nutritional status in patients with liver cirrhosis, *Gastroenterology Research and Practice* 4 (2017)1-10, <https://doi.org/10.1155/2017/6765856>.
- [7] C. Busse, P. Biechele, I. de Vries, K.F. Reardon, D. Solle, T. Scheper, Sensors for disposable bioreactors, *Eng. Life. Sci.* 17 (2017) 940-952, [https://DOI: 10.1002/elsc.201700049](https://doi.org/10.1002/elsc.201700049).
- [8] J-G. Guan, Y-Q. Miao, Q-J. Zhang, Impedimetric Biosensors. *J. Biosci. Bioeng.* 97 (2004) 219–226, doi.org/10.1016/j.bioelechem.2020.107632.
- [9] Y. Kim, Y. J. Park, H. Jung, An impedimetric biosensor for real-time monitoring of bacterial growth in a microbial fermentor. *Sensors Actuators B: Chem.* 138 (2009) 270-277, <https://doi.org/10.1016/j.snb.2009.01.034>.
- [10] G.H. Markx, C.L.Davey, The dielectric properties of biological cells at radiofrequencies: applications in biotechnology, *Enzyme. Microb. Technol.* 25 (1999)161-171, [https://doi.org/10.1016/S0141-0229\(99\)00008-3](https://doi.org/10.1016/S0141-0229(99)00008-3).
- [11] P. Patel, G.H. Markx, Dielectric measurement of cell death, *Enz. Microb. Technol.* 42 (2008) 463-470, <https://doi.org/10.1016/j.enzmictec.2008.09.005>.

- [12] N. Nasir, M Al Ahmad, Cells Electrical Characterization: Dielectric Properties, Mixture, and Modeling Theories, J. Engineer. 2020 (2020) Article ID 9475490, <https://doi.org/10.1155/2020/9475490>.
- [13] K. Heileman, J. Daoud, M. Tabrizian, Dielectric spectroscopy as a viable biosensing tool for cell and tissue characterization and analysis. Biosens Bioelectron 49 (2013) 348-359, <https://doi.org/10.1016/j.bios.2013.04.017>.
- [14] R.D. Stoy, K. R. Foster, H. P. Schwan, Dielectric properties of mammalian tissues from 0.1 to 100 MHz: a summary of recent data. Phys Med Biol. 27 (1982) 501-513, doi: 10.1088/0031-9155/27/4/002.
- [15] C. Prodan, F. Mayo, J.R. Claycomb, J.H. Miller Jr., Low-frequency, low-field dielectric spectroscopy of living cell suspensions, J. Appl. Phys. 95 (2004) 3754–3756, <https://doi.org/10.1063/1.1649455>.
- [16] C. Prodan, E. Prodan. 1999. The dielectric behaviour of living cell suspensions. J. Phys. D: Appl. Phys. 32 (1999) 335-343.
- [17] A.L. Martin, P. Satjaritanun, S. Shimpalee, B.A.Devivo, J. Weidner, S. Greenway, J.M. Henson, C.E. Turick, In-situ electrochemical analysis of microbial activity, Appl. Microbiol. Biotechnol. Exp. 8 (2018) 162, <https://doi.org/10.1186/s13568-018-0692-2>.
- [18] E. Marsili, J B Rollefson, D. B. Baron, R. M. Hozalski, D. R. Bond, Microbial biofilm voltammetry: direct electrochemical characterization of catalytic electrode-attached biofilms. Appl. Environ. Microbiol. 74 (2008) 7329-7337, doi:10.1128/AEM.00177-08.
- [19] C. E. Turick, A. Beliaev, A. A. Ekechukwu, T. Poppy, A. Maloney, D. A. Lowy, The role of 4-hydroxyphenylpyruvate dioxygenase in enhancement of solid-phase electron transfer by *Shewanella oneidensis* MR-1. FEMS Microbiology Ecology. 68 (2009) 223- 235, DOI:[10.1111/j.1574-6941.2009.00670.x](https://doi.org/10.1111/j.1574-6941.2009.00670.x).
- [20] F. Kracke, I. Vassilev, J. O. Krömer, Microbial electron transport and energy conservation – the foundation for optimizing bioelectrochemical systems. Front. Microbiol. 6 (2015) 575, doi: 10.3389/fmicb.2015.00575.
- [21] C. E. Turick, F. Caccavo Jr., L. S. Tisa, Electron transfer to *Shewanella algae* BrY to HFO is mediated by cell-associated melanin, FEMS Microbiol. Let. 220 (2003) 99-104, [https://doi.org/10.1016/S0378-1097\(03\)00096-X](https://doi.org/10.1016/S0378-1097(03)00096-X).
- [22] V. M. Cimpoiasu, R. Popa. Capsule-bound pyomelanin as an electrical conduit in *Shewanella oneidensis* MR-1. Physics AUC. 29 (2019) 25-35.
- [23] I. Weidenfeld, C. Zakian, P. Duewell, A. Chmyrov, U. Klemm, J. Aguirre, V. Ntziachristos, A. C. Stiel. Homogentisic acid-derived pigment as a biocompatible label

- p>for optoacoustic imaging of macrophages. Nat. Commun. 10 (2019) 5056,
-
- doi.org/10.1038/s41467-019-13041-4.
- [24] E. C. Howard, L. J. Hamdan, S. E. Lizewski, B. R. Ringeisen, High frequency of glucose-utilizing mutants in *Shewanella oneidensis* MR-1, *FEMS Microbiology Letters*, 327 (2012) 9 –14, <https://doi.org/10.1111/j.1574-6968.2011.02450.x>.
 - [25] F. Palmisano, P. G. Zambonin, D. Centonze, M. Quinto, A disposable, reagentless, third-generation glucose biosensor based on overoxidized poly(pyrrole)/tetrathiafulvalene tetracyanoquinodimethane composite. *Anal. Chem.* (2002) 5913-5918, <https://doi.org/10.1021/ac0258608>.
 - [26] C. Zhang, L. Slater, C. Prodan, Complex dielectric properties of sulfate-reducing bacteria suspensions. *Geomicrobiol. J.* 30 (2013) 490-496, <https://doi.org/10.1080/01490451.2012.719997>.
 - [27] R. Gómez-Sjöberg, D. T. Morissette, R. Bashir. Impedance microbiology-on-a-chip: microfluidic bioprocessor for rapid detection of bacterial metabolism. *J. Microelectromechanical Syst.* 14 (2005) 829-838, DOI: [10.1109/JMEMS.2005.845444](https://doi.org/10.1109/JMEMS.2005.845444).
 - [28] K.S. Cole, R.H. Cole, Dispersion and absorption in dielectrics - II direct current characteristics. *J Chem Phys* 10 (1942) 98–105, <https://doi.org/10.1063/1.1723677>.
 - [29] C.E. Turick, L. S. Tisa, F. Caccavo Jr., Melanin production and use as a soluble electron shuttle for Fe (III) oxide reduction and as a terminal electron acceptor by *Shewanella algae* BrY. *Appl. Environ. Microbiol.* 68 (2002) 2436–2444, DOI: [10.1128/AEM.68.5.2436-2444.2002](https://doi.org/10.1128/AEM.68.5.2436-2444.2002).
 - [30] C.L. Slayman, C. W. Slayman, Depolarization of the plasma membrane of *Neurospora* during active transport of glucose: evidence for a proton-dependent cotransport system. *Proc. Nat. Acad. Sci.* 71 (1974) 1935-1939, <https://doi.org/10.1073/pnas.71.5.1935>.
 - [31] G. Z. Abdel Aal, A.E. Atekwana, S. Rossbach, D.D. Werkema, Sensitivity of geochemical measurements to the presence of bacteria in porous media. *J Geophys Res* 115 (2010) G03017, <https://doi.org/10.1029/2009JG001279>.
 - [32] R. Gómez, R. D. Akin, A. K. Bhunia, M. R. Ladisch, R. Bashir. Microscale impedance-based detection of bacterial metabolism. *Proceedings of the 7th internat. Conf. Miniaturized Chem. and Biochem. Anal. Sys.* Oct.5-9, (2003) Squaw Valley, CA, USA. pp 1227-1230.
 - [33] G. Z. Abdel Aal, E. A. Atekwana, E. A. Atekwana, Effect of bioclogging in porous media on complex conductivity signatures. *J Geophys Res* 115 (2010) G00G07, DOI: [10.1029/2009JG001159](https://doi.org/10.1029/2009JG001159).

- [34] A. Mella, C.M. Smeaton, A. Furman, E.A. Atekwana, F. Rezanezhad, P.V. Cappellen, Linking spectral induced polarization (SIP) to subsurface microbial processes; results from sand column incubation experiments. *Environ. Sci. Technol.* 52 (2018) 2081-2090, <https://doi.org/10.1021/acs.est.7b04420>.
- [35] D. Ntarlagiannis, A. Ferguson, SIP response of artificial biofilms, *Geophysics* 74 (2008) A1–A5, <https://doi.org/10.1190/1.3031514>.
- [36] S. Pirbadian, M.S. Chavez, M.Y. El-Naggar. Spatiotemporal mapping of bacterial membrane potential responses to extracellular electron transfer, *PNAS*, 117 (2020) 20171-20179, doi:10.1073/pnas.2000802117.
- [37] Y. Hubenova, E. Hubenova, M. Mitov, Electroactivity of the Gram-positive bacterium *Paenibacillus dendritiformis* MA-72. *Bioelectrochemistry*, 136 (2020)107632, <https://doi.org/10.1016/j.bioelechem.2020.107632>.
- [38] H. von Canstein, J. Ogawa, S. Shimizu, J. R. Lloyd, Secretion of Flavins by *Shewanella* Species and Their Role in Extracellular Electron Transfer. *Appl. Environ. Microbiol.* 74 (2008) 615– 623, doi: [10.1128/AEM.01387-07](https://doi.org/10.1128/AEM.01387-07).
- [39] R.P. Ramasamy, V. Gadhamshetty, L.J. Nadeau, G.R. Johnson, Impedance spectroscopy as a tool for non-intrusive detection of extracellular mediators in microbial fuel cells, *Biotechnol. Bioeng.* 104 (2009) 882–891, <https://doi.org/10.1002/bit.22469>.
- [40] D.K. Newman, R.A. Kolter, A role for excreted quinones in extracellular electron transfer. *Nature* 405 (2000) 94-97, doi: 10.1038/35011098. PMID: 10811225.
- [41] E.D. Brutinel, J. A. Gralnick, Shuttling happens: soluble flavin mediators of extracellular electron transfer in *Shewanella*. *Appl. Microbiol. Biotechnol.* 93 (2012) 41–48, <https://doi.org/10.1007/s00253-011-3653-0>.
- [42] N.J. Kotloski, J. A. Gralnick, Flavin Electron Shuttles Dominate Extracellular Electron Transfer by *Shewanella oneidensis*, *mBio*. 4 (2013) e00553-12, <https://doi.org/10.1128/mBio.00553-12>.
- [43] A.J. Grimbergen, J. Siebring, A. Solopova, O. P. Kuipers, Microbial bet-hedging: the power of being different. *Current Opinion in Microbiology*, 25 (2015) 67–72, <https://doi.org/10.1016/j.mib.2015.04.008>.
- [44] V. Takhaveev, M. Heinemann, Metabolic heterogeneity in clonal microbial populations, *Current Opinion in Microbiology*, 45 (2018) 30–38, <https://doi.org/10.1016/j.mib.2018.02.004>.
- [45] A.T. Bull, The renaissance of continuous culture in the post-genomics age. *J. Ind. Microbiol. Biotechnol.* 37 (2010) 993–1021, <https://doi.org/10.1007/s10295-010-0816-4>.

- [46] R.G. Arnold, T. J. DiChristina, M. R. Hoffmann, Inhibitor studies of dissimilative Fe(III) reduction by *Pseudomonas* sp. Strain 200 ("*Pseudomonas ferrireductans*"). Appl. Environ. Microbiol. 52 (1989) 281-289, DOI:<https://doi.org/10.1128/aem.52.2.281-289.1986>.
- [47] S. Detchanamurthy, P. A. Gostomski, Metabolic uncouplers in environmental research: a critical review. Rev. Chem. Eng. 28 (2012) 309–317, <https://doi.org/10.1515/revce-2012-0004>.
- [48] J.E. Hobbie, R. J. Daley, S. Jasper. Use of Nuclepore Filters for Counting Bacteria by Fluorescence Microscopy. Appl. Environ. Microbiol. 33 (1977) 1225-1228, <https://doi.org/10.1128/aem.33.5.1225-1228.1977>.

Figure Legends

Figure 1. Circuit model. The equivalent circuit used to fit the data where R1 represents electrolyte resistance at high frequency, CPE1 and R2 represent a constant phase element and charge transfer resistance, respectively at lower to medium frequencies, with CPE2 and R3 representing a constant phase element and a modification of the charge transfer resistance respectively at low to high frequencies.

Figure 2. Growth study. *S. oneidensis* $\Delta hmgA$ (a), and *S. oneidensis* $\Delta melA$ (b) grown in BHM + glucose, demonstrated physiological activity based on oxygen utilization (—■—) during growth. Supplementation of glucose (··●··) at the beginning and at 42 h (red arrows) correlated with increased physiological activity based on oxygen utilization and glucose depletion. Cell densities (◆) of $\Delta hmgA$ (c), and $\Delta melA$ (d) correlated with CO₂ yield (—●—) during growth and followed glucose utilization. Error bars represent standard deviation.

Figure 3. Effects of growth on phase angle (ϕ). $\Delta\phi$ of *S. oneidensis* $\Delta hmgA$ (a), and *S. oneidensis* $\Delta melA$ (b) demonstrated peaks between 1 Hz and 10 kHz during growth studies with peak heights generally increasing during growth and peak frequency varying with time and glucose concentration. Selected times are presented here for clarity.

Figure 4. Peak heights and frequencies of $\Delta\phi$ during growth of *S. oneidensis* $\Delta hmgA$ (a), and *S. oneidensis* $\Delta melA$ (b). Maximum peak heights increased following initial addition of glucose (first red arrow) with sharp declines immediately following supplementation of glucose (second red arrow). Peak frequencies gradually declined during glucose utilization followed by sudden increases in response to glucose supplementation. Inset graphs demonstrate the correlation of $\Delta\phi$ maximum peak heights and cell density.

Figure 5. CO₂ yield (●) and real, relative permittivity ($\Delta\epsilon'/\epsilon_0$) (■) during growth of *S. oneidensis* $\Delta hmgA$ (a), and *S. oneidensis* $\Delta melA$ (b). Real relative permittivity followed a general trend of CO₂ yield, indicating a link to metabolic activity. A sudden drop of metabolic activity after 45 h by *S. oneidensis* $\Delta melA$ (b) correlated to decreased metabolic viability.

Figure 6. Effects of growth on admittance (Y''). $\Delta Y''$ of *S. oneidensis* $\Delta hmgA$ (a), and *S. oneidensis* $\Delta melA$ (b) demonstrated peaks between 1 Hz and 100 Hz during growth studies where peak heights generally increased during growth. Peak frequency varied with time and glucose concentration. Selected times are presented here for clarity.

Figure 7. Peak heights and frequencies of $\Delta Y''$ during growth of *S. oneidensis* $\Delta hmgA$ (a), and *S. oneidensis* $\Delta melA$ (b). Maximum peak heights and frequencies gradually declined following initial addition of glucose (first red arrow) with sharp increases immediately following supplementation of glucose (second red arrow).

Figure 8. Nyquist plots of impedance during growth of $\Delta hmgA$ (a) and $\Delta melA$ (b). Selected times are presented here for clarity. Higher frequency data (indicated in dashed square) are shown in the insets. Data at 42 h (before glucose supplementation) and 45 h (after glucose

supplementation) are depicted with dashed lines to demonstrate the decrease in charge transfer resistance after glucose addition. A greater degree of charge transfer resistance was demonstrated by *ΔmelA*, as well as an increase in charge transfer resistance after the glucose addition.

Figure 9. Cole-Cole plots of permittivity during growth of *ΔhmgA* (a) and *ΔmelA* (b). Selected times are presented here for clarity. Data at 42 h (before glucose supplementation) and 45 h (after glucose supplementation) are depicted with dashed lines to demonstrate the temporary decrease in permittivity after glucose addition. A greater degree of charge transfer resistance was demonstrated by *ΔmelA*.

Figure 10. Log₁₀ values of R1 Determined by fitting impedance data to the equivalent circuit. Circuit element R1 represents the resistances from current flowing through the solution outside of the microbes. Aside from slight changes in values of *S. oneidensis ΔhmgA* (black squares) up to the first 16 h compared to that of *S. oneidensis ΔmelA* (red circles) the solution currents varied little.

Figure 11. Log₁₀ values of R2 based on data fitting to the equivalent circuit. R2 values of *S. oneidensis ΔhmgA* (black squares) spiked initially followed by relatively stable values during growth. However, R2 values of *S. oneidensis ΔmelA* (red circles) were consistently several logs higher than those of *S. oneidensis ΔhmgA*. These values corresponded generally to carbon and energy source concentrations.

Figure 12. Values of R3 determined by fitting impedance data to the equivalent circuit with *S. oneidensis ΔhmgA* (black line and squares) and *S. oneidensis ΔmelA* (red line and circles). Circuit element R3 represents the charge transfer resistance and was greater for *S. oneidensis ΔmelA*. For both cultures, R3 values increased as the electron source (glucose) decreased. When glucose was supplemented at 42 h, the charge transfer resistance decreased for both cultures. *S. oneidensis ΔmelA* demonstrated physiological stress which resulted in fluctuations in R3.

Figure 13. Fitting results for the two constant phase elements (CPEs) present in the equivalent circuit model. CPE1 and CPE2 are split into two components, the T component representing the capacitance contribution and the P component representing the phase contribution for the CPEs

Figure 14. Cyclic voltammograms. Selected voltammograms of *S. oneidensis ΔhmgA* (black line) and *S. oneidensis ΔmelA* (red line) demonstrated various redox characteristics of the cultures throughout the growth study at 24 h (0 h, inset) (a); 42 h, prior to glucose supplementation (b); 52 h, just after glucose supplementation (c) and 62 h (d).

Figures

Figure 1.

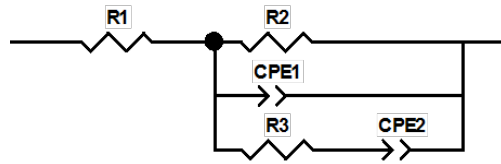


Figure 2

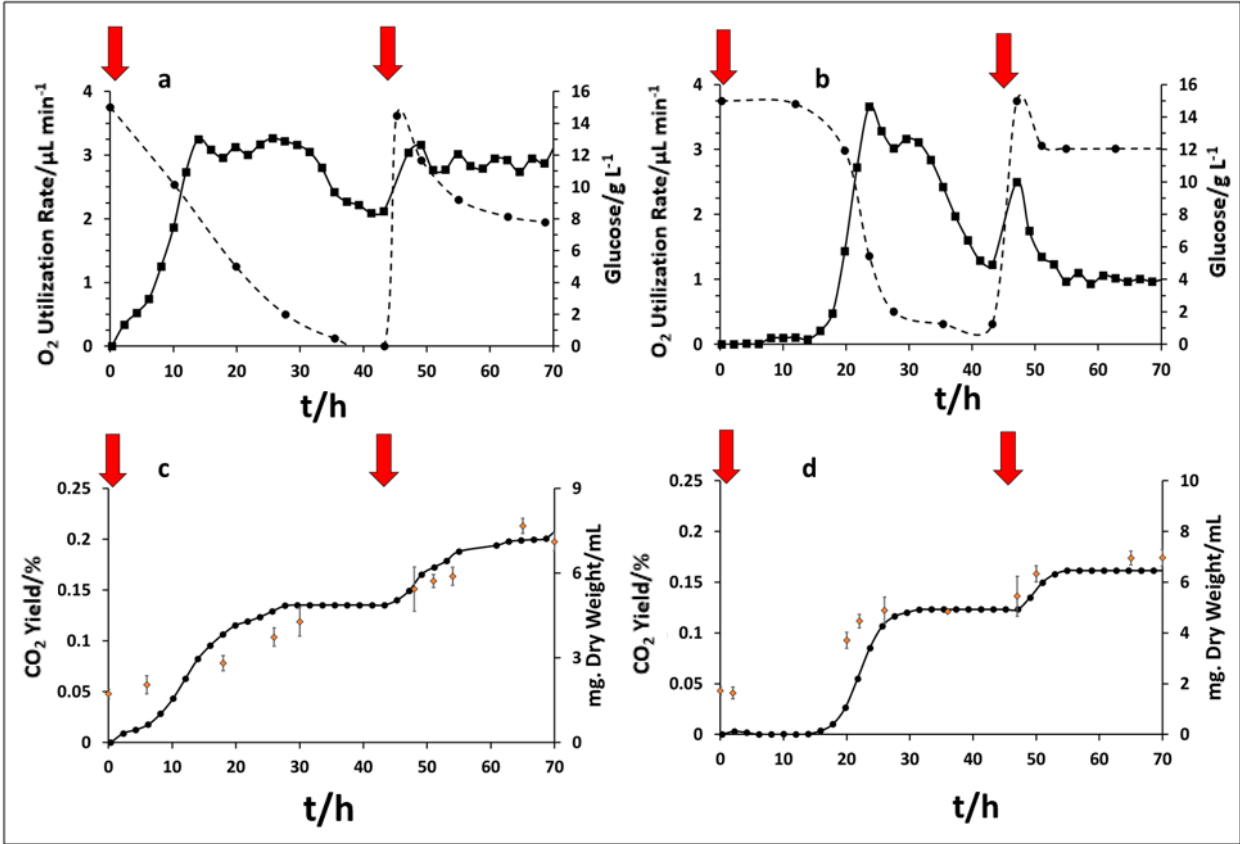


Figure 3.

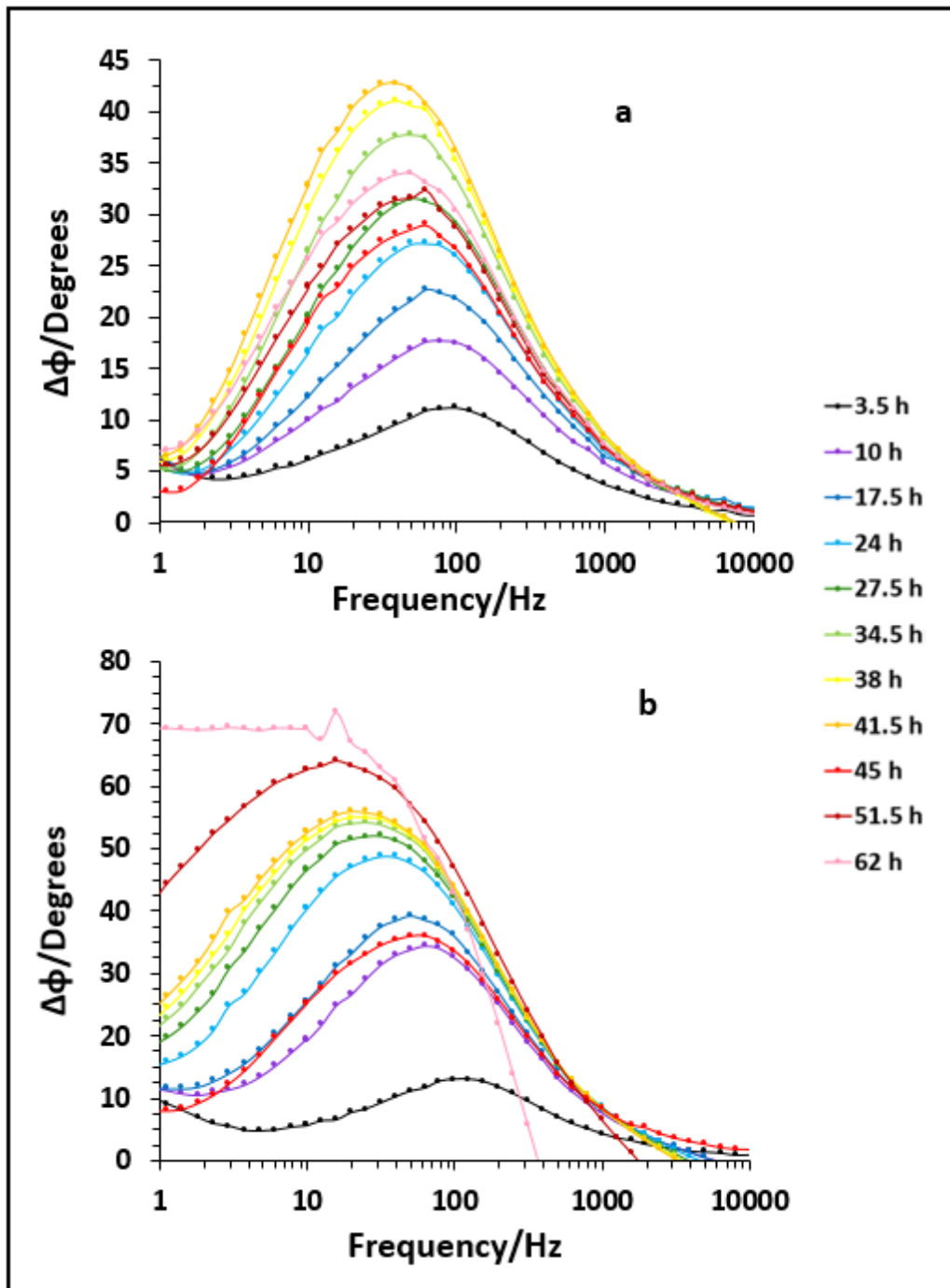


Figure 4.

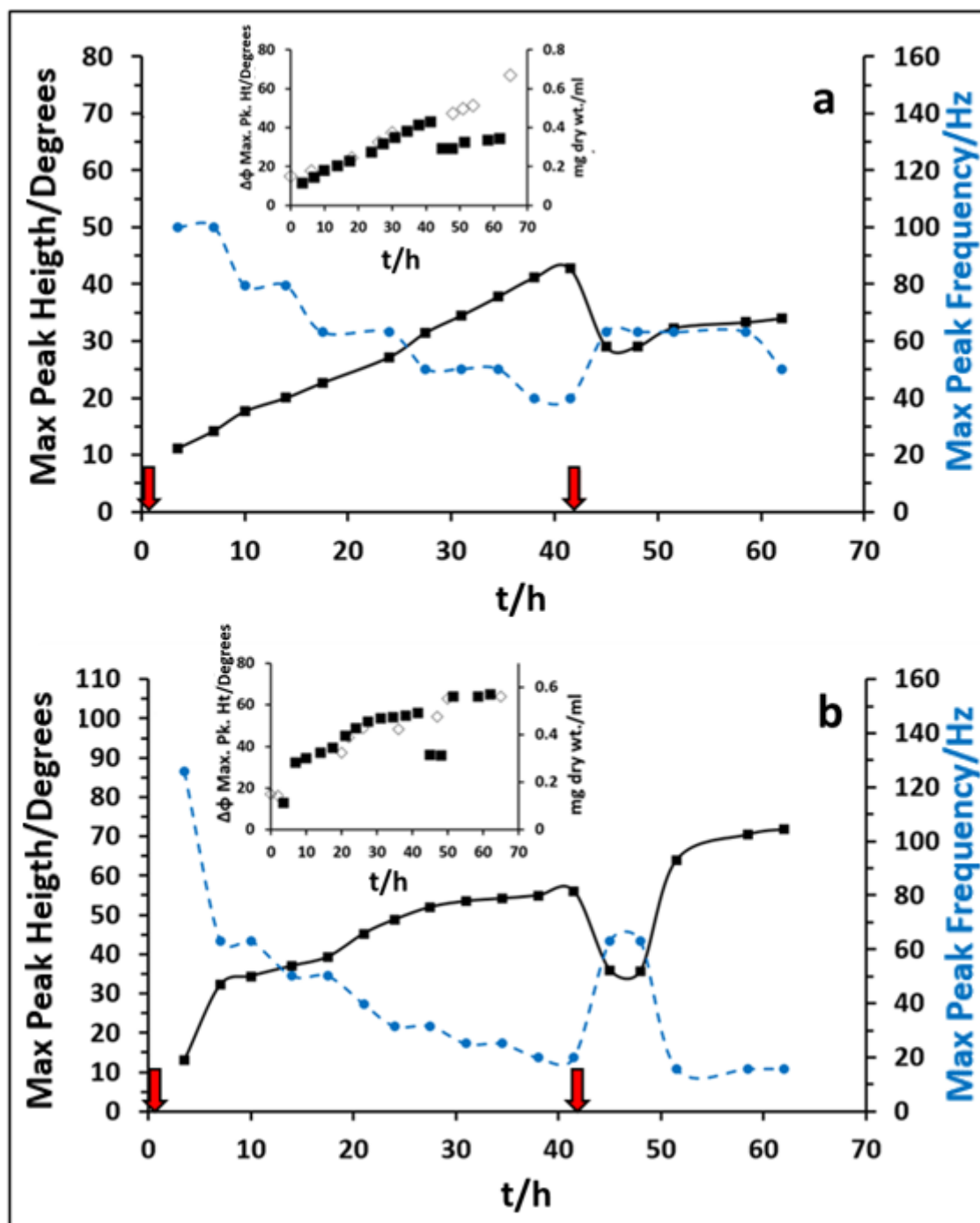


Figure 5.

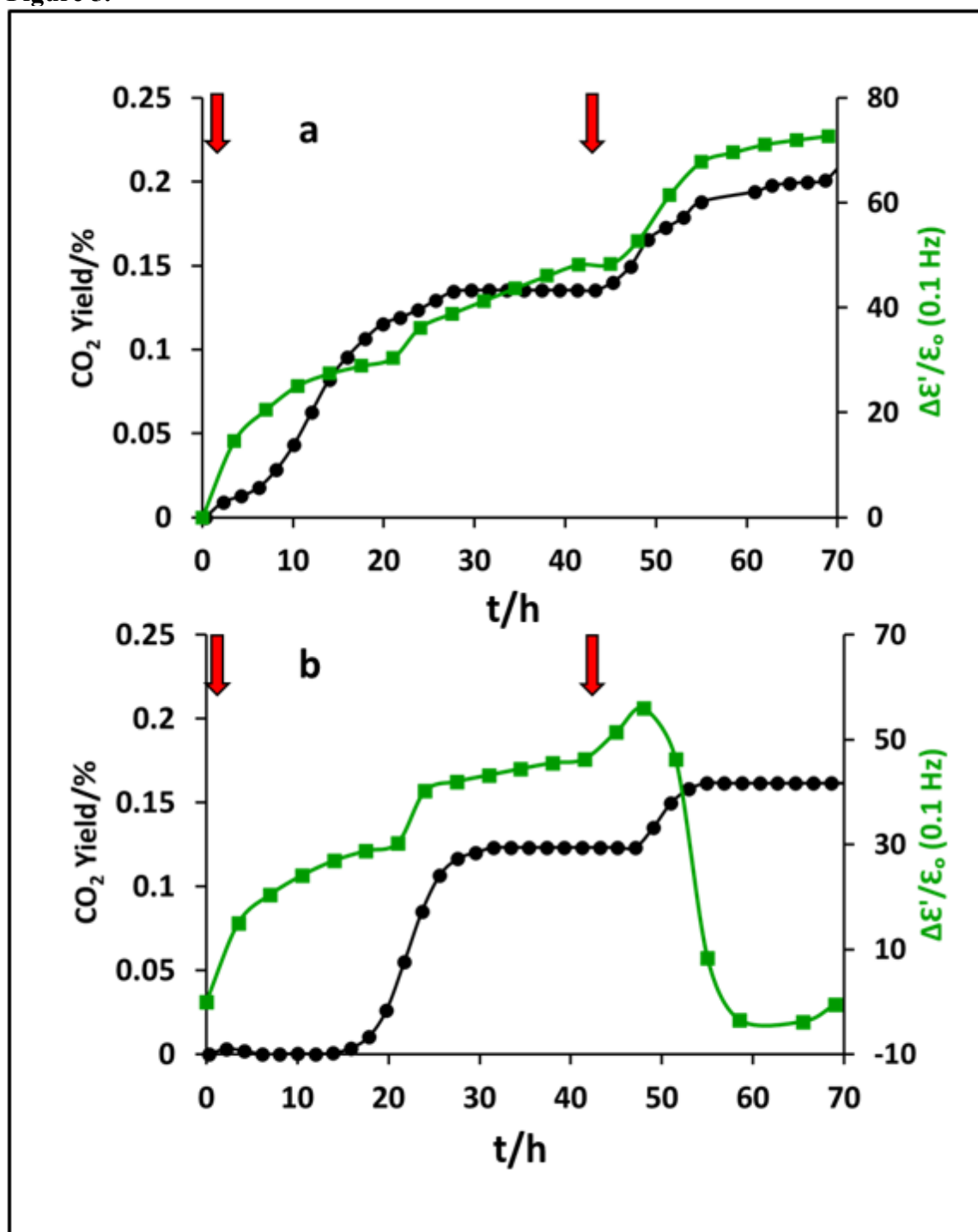


Figure 6.

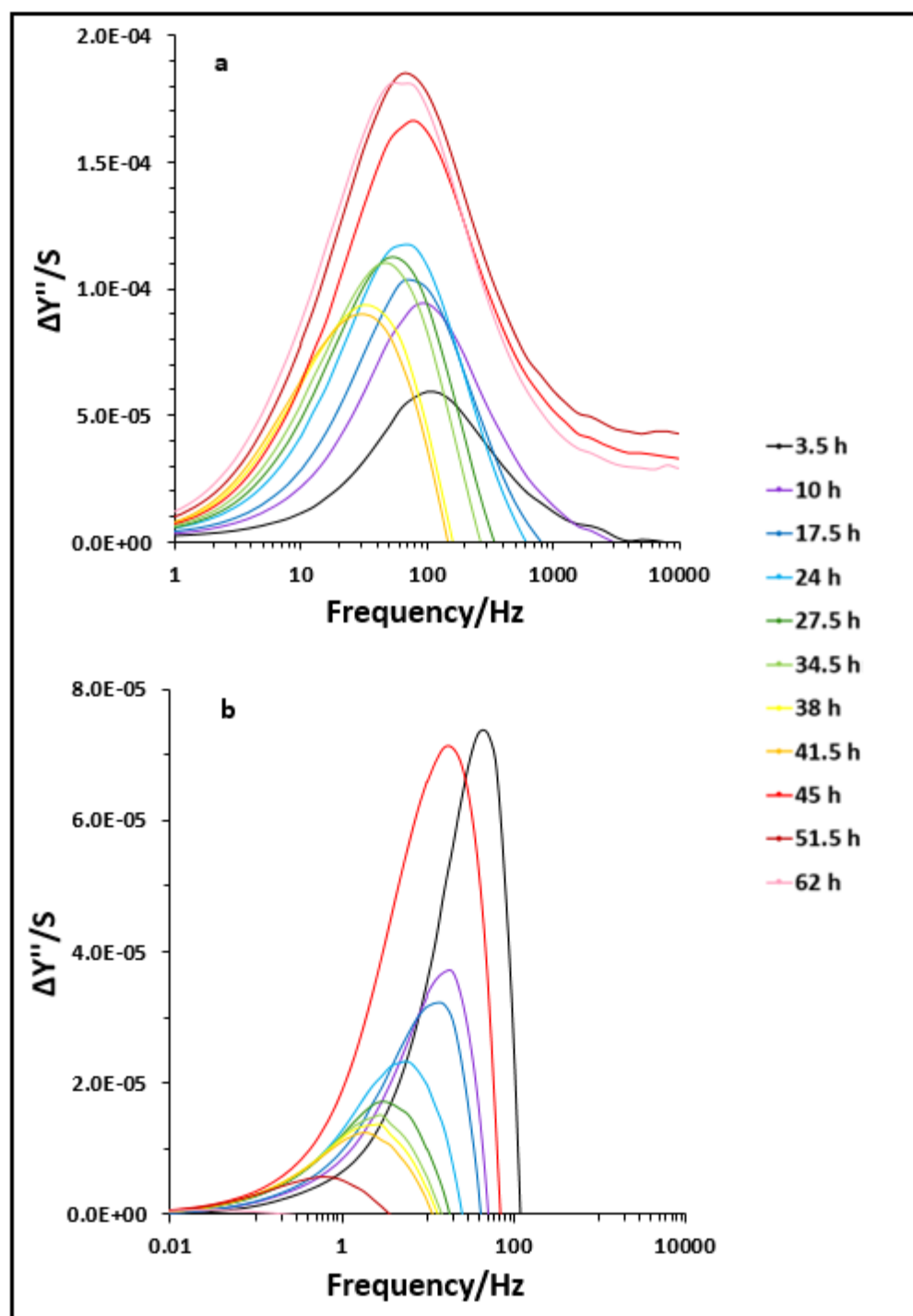


Figure 7.

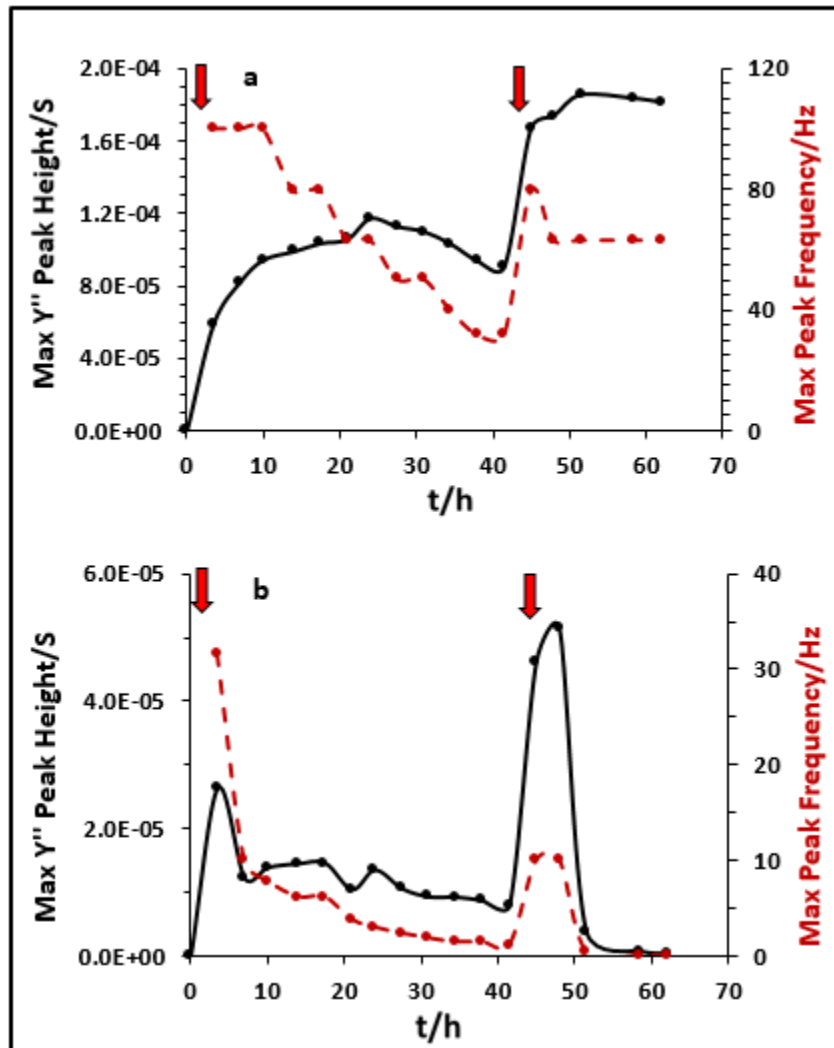


Figure 8.

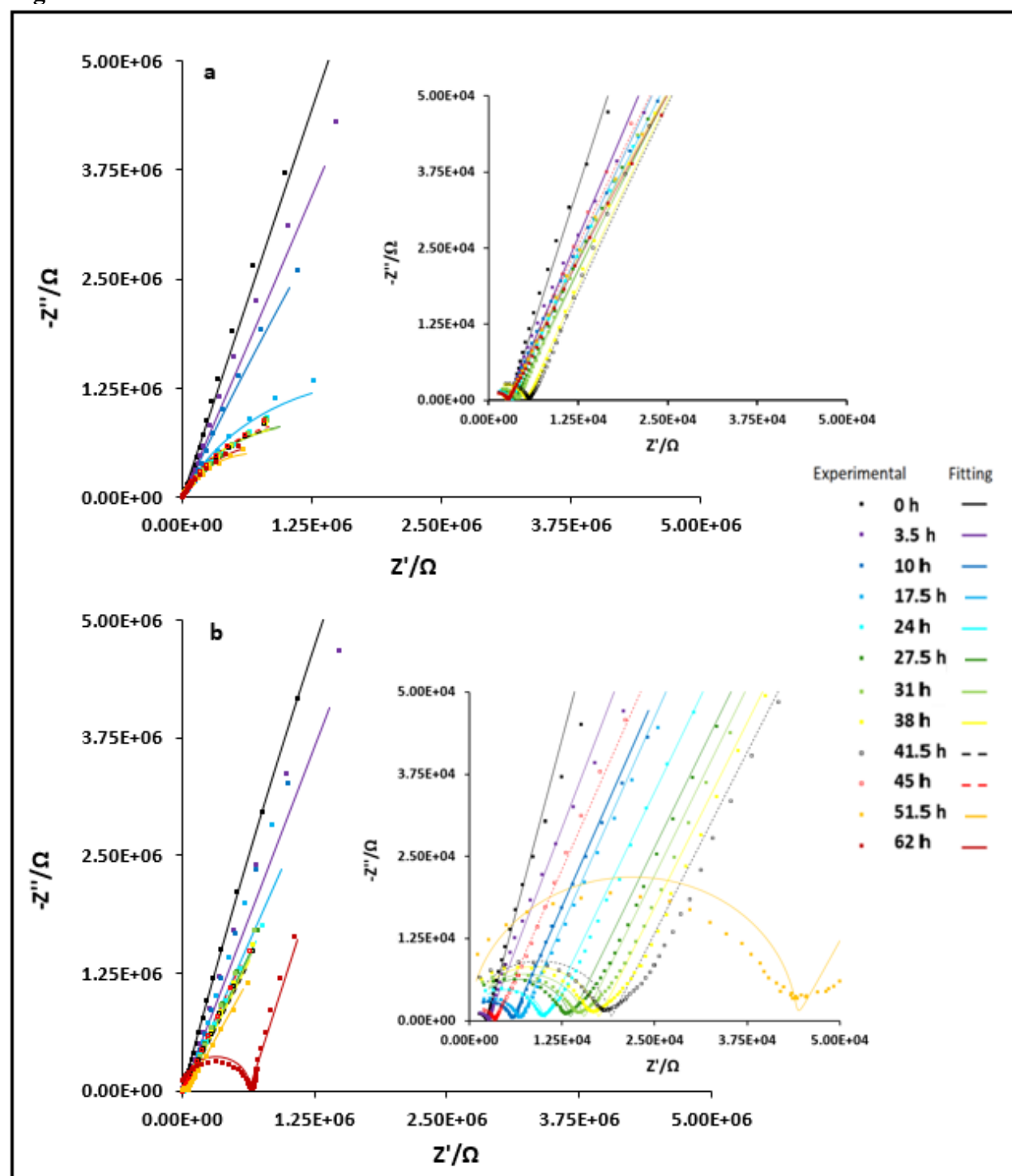


Figure 9.

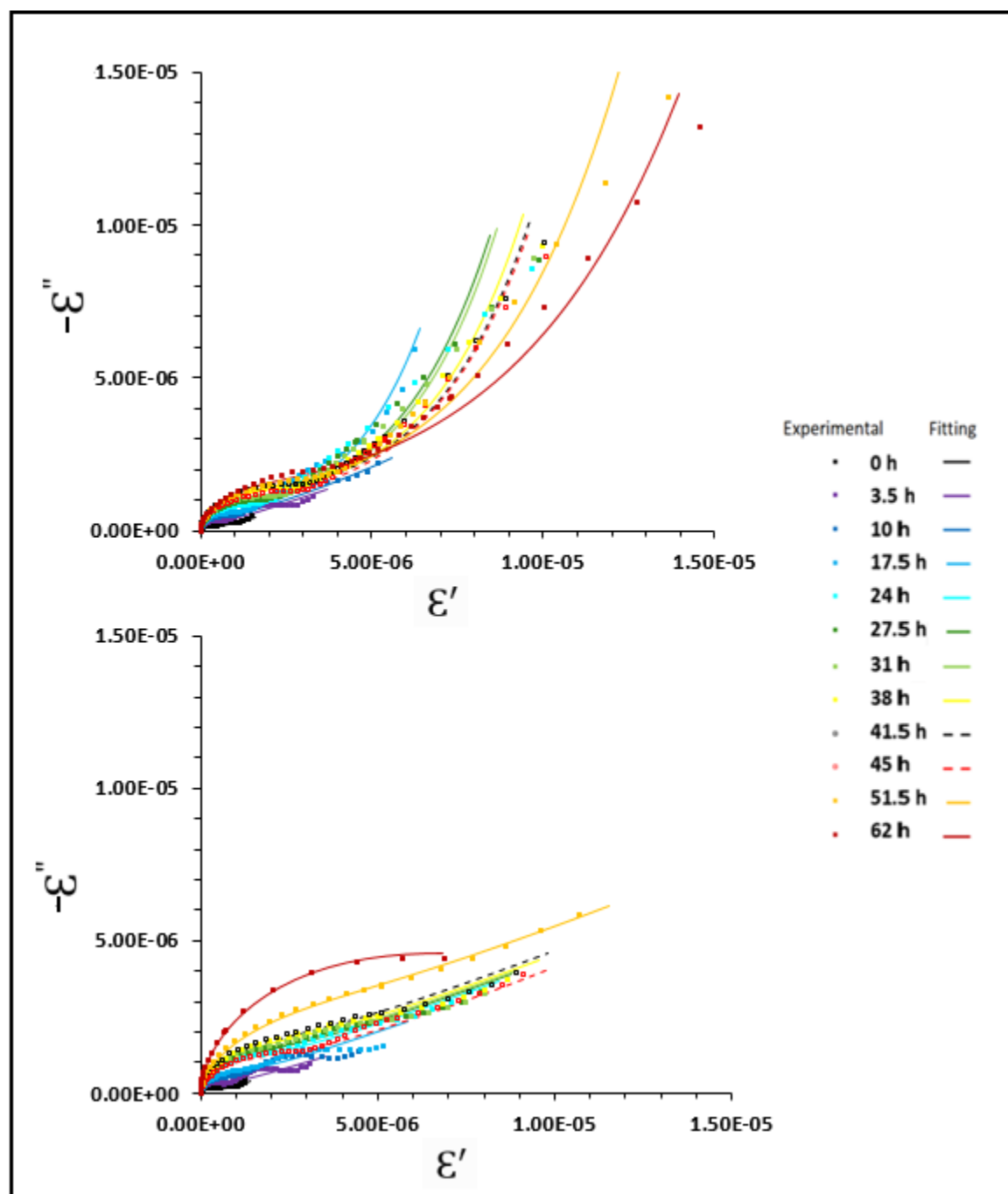


Figure 10.

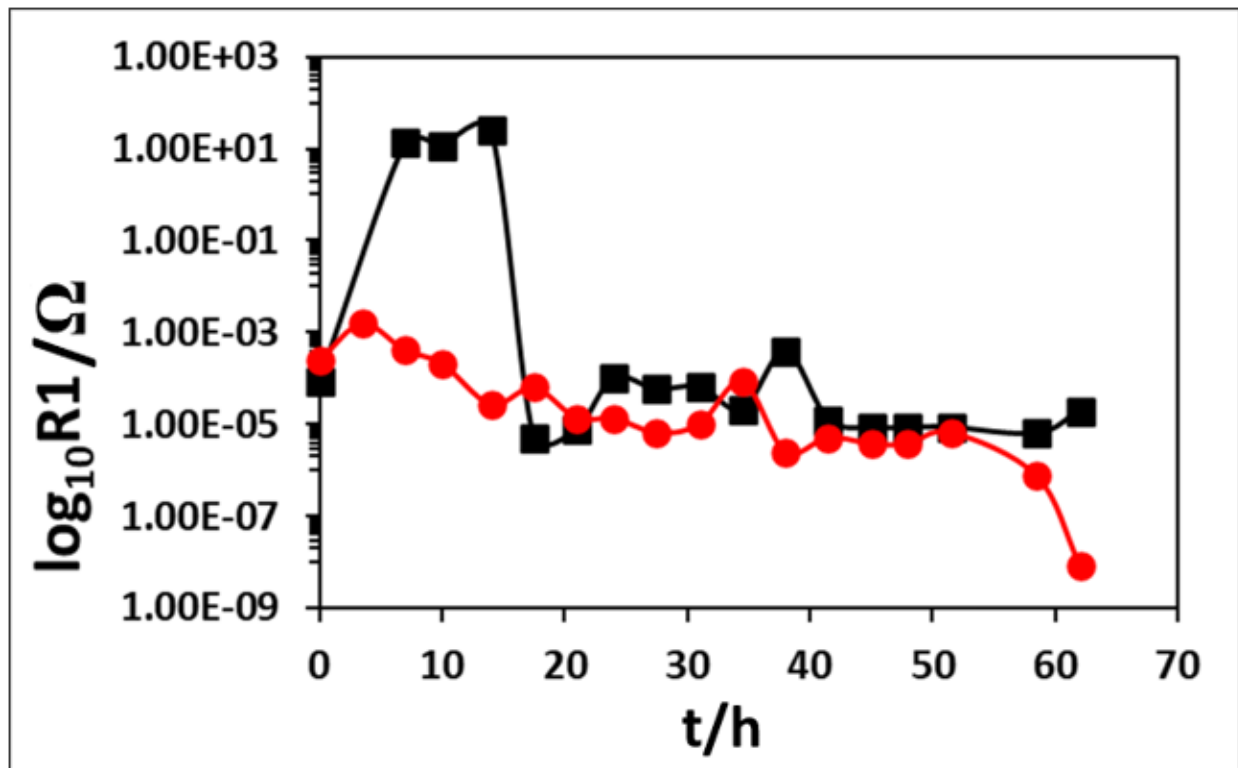


Figure 11.

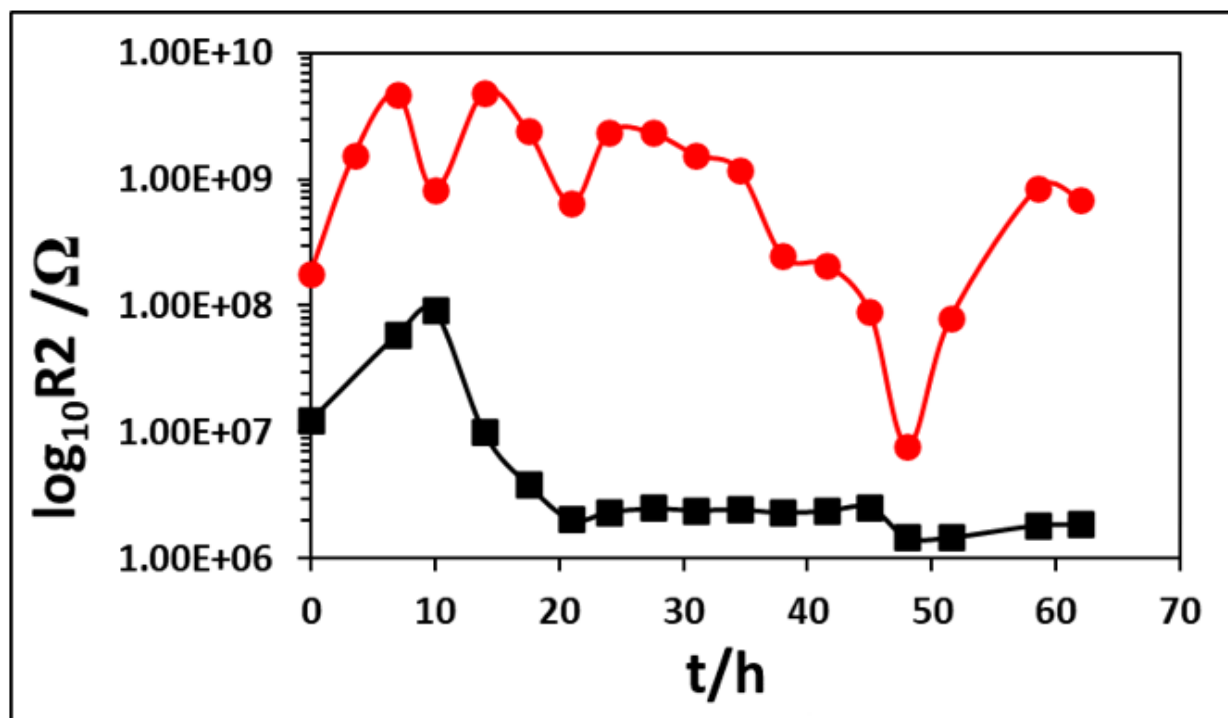


Figure 12.

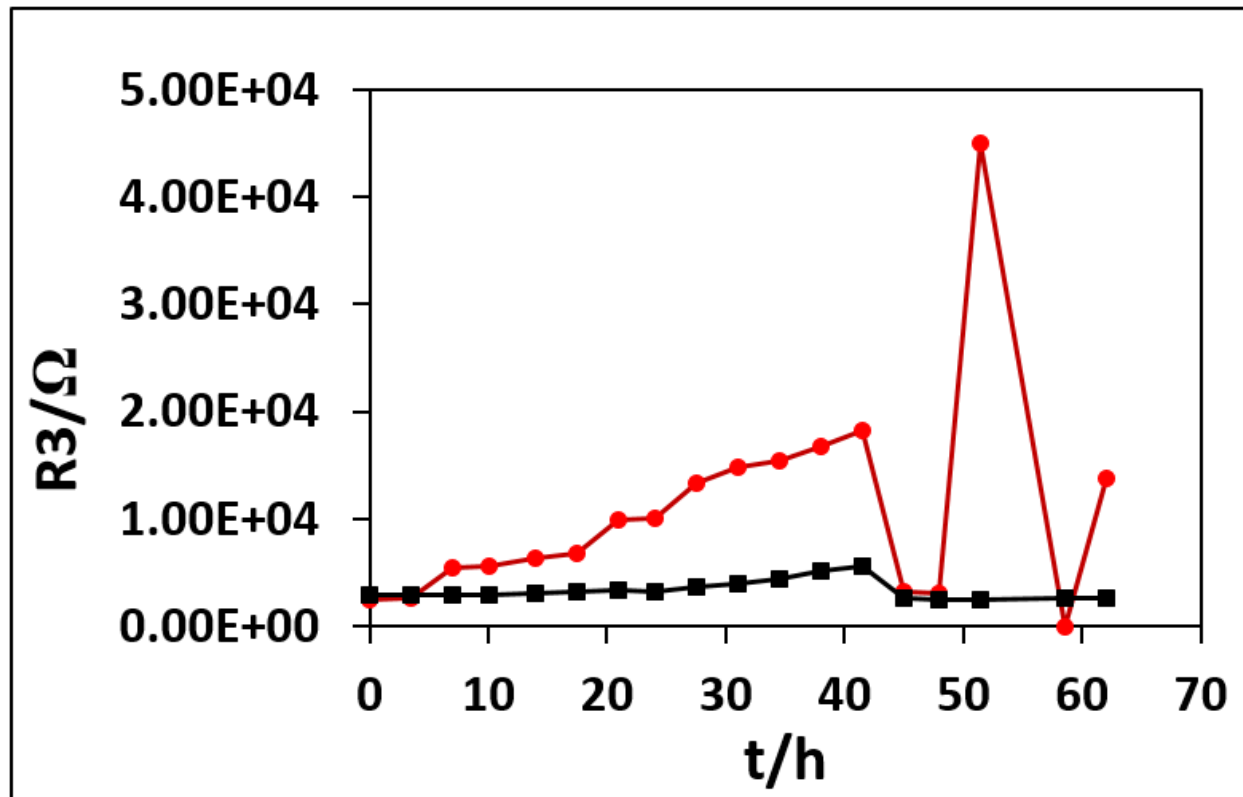


Figure 13.

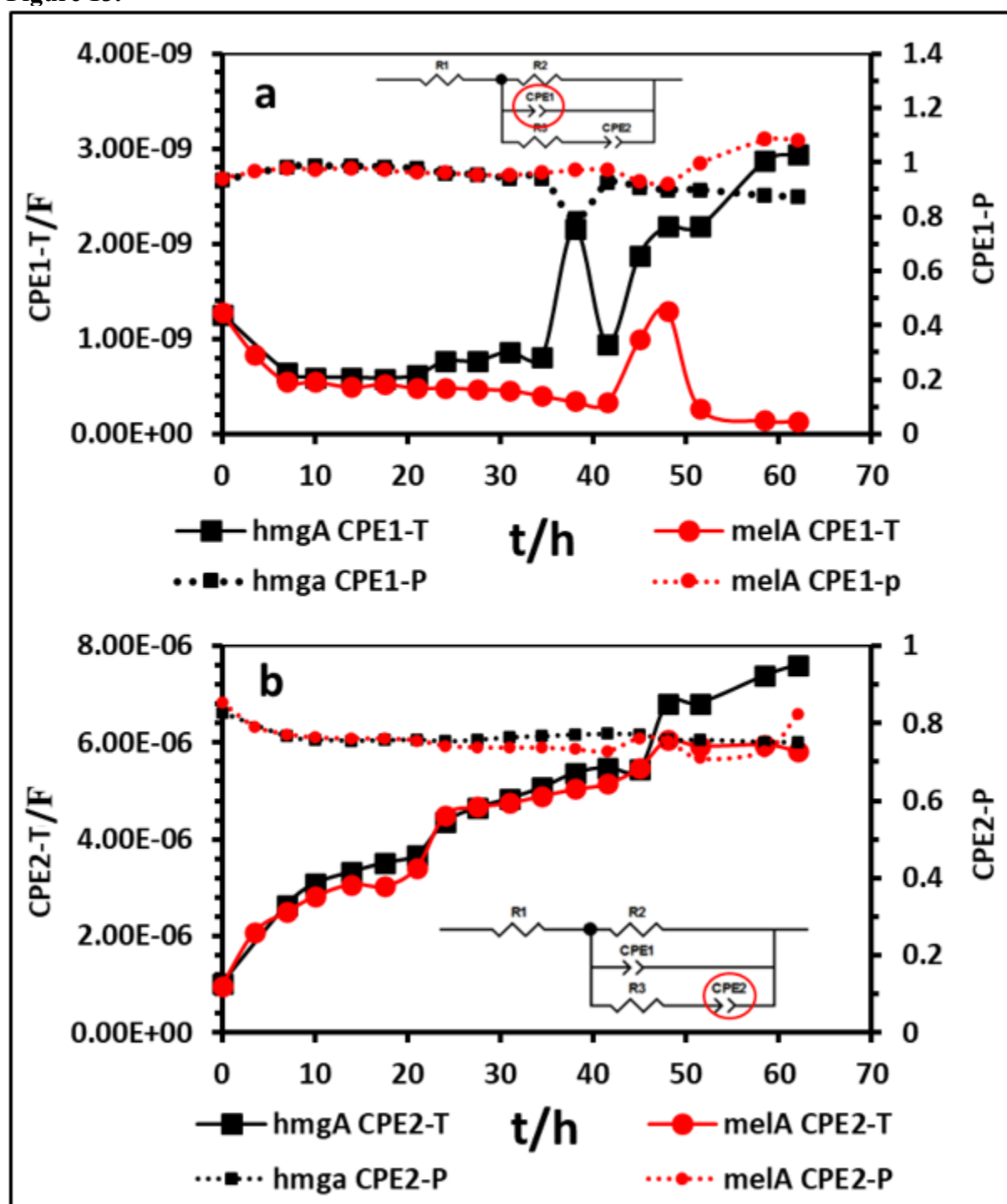


Figure 14.

